

Experimental prospects at the Large Hadron Collider*

Daniel Froidevaux¹ and Vasiliki A Mitsou²

¹ CERN, PH Department, CH-1211 Geneva 23, Switzerland

² Instituto de Física Corpuscular (IFIC), CSIC – Universitat de València, Apartado de Correos 22085, E-46071 Valencia, Spain

Abstract. This review focuses on the expected performance of the ATLAS and CMS detectors at the CERN Large Hadron Collider (LHC), together with some of the highlights of the global commissioning work done in 2008 with basically fully operational detectors. A selection of early physics measurements, expected to be performed with the data taken in 2009/2010 is included for completion, together with a brief reminder of the ultimate physics potential of the LHC.

1. Introduction

The Large Hadron Collider (LHC) [1], located at CERN, the European Laboratory for Particle Physics, outside Geneva, Switzerland, will hopefully see its first collisions at a centre-of-mass energy of 10 TeV towards the end of 2009. In September 2008, excitement reached its peak after a very successful start-up of the machine with single beams, but an unfortunate incident caused substantial damage in one of the sectors of the machine and delayed the first collisions by about one year.

The LHC accelerator complex and its experiments will provide a long-awaited and unprecedented tool for fundamental physics research for many years to come. Ultimately, the LHC will provide two proton beams, circulating in opposite directions, at their design energy of 7 TeV each, corresponding to a centre-of-mass energy of $\sqrt{s} = 14$ TeV), and at a design luminosity of 10^{34} cm⁻²s⁻¹. The two general-purpose experiments, ATLAS (A Toroidal LHC ApparatuS) [2] and CMS (Compact Muon Solenoid) [3], share a long and common history: they were conceived in the early 90's at the same time as a world-wide Research and Development effort began, focused on the numerous technical challenges associated with operation in the harsh environment of the LHC. They were approved in 1994, the detailed design of the various parts of the apparatus was completed and reviewed between 1997 and 2002, the construction proceeded between 1997 and 2007, and the integration and installation at CERN was finally completed during the summer of 2008. The experiments were therefore ready just in time for first beams in the fall of 2008. Next year is therefore hopefully going to see the culmination of the work of thousands of people across the world over almost twenty years.

* In this review, only the detector and physics performance of ATLAS and CMS, the two general-purpose experiments at the Large Hadron Collider, will be addressed. Two other large experiments, namely LHCb [4] and ALICE [5], dedicated to B-physics and heavy ions, respectively, will also operate at the LHC. Finally TOTEM [6] and LHCf [7] will focus on forward physics at the LHC.

2. ATLAS/CMS: from design to reality

In the following, the basic requirements which drove the design of the ATLAS and CMS detectors, the technological choices adopted by the collaborations, and the performance expected for the measurement and identification of the major physics objects are reviewed.

2.1. An unprecedented scale and complexity

The constraints of the unprecedented energy and luminosity of the LHC accelerator have led to detectors, which are colossal in many aspects and of considerable complexity in many others:

Size of detectors With a volume of 20 000 m³, ATLAS is one of the largest accelerator-based experiments built so far, while CMS is one of the heaviest, weighing 12 500 tons. Both detectors feature 70 to 80 million pixel readout channels near the interaction point. The active silicon of the CMS tracker covers 200 m², whereas the ATLAS liquid argon (LAr) electromagnetic (EM) calorimeter contains a total of 175 000 readout channels. For the detection and momentum measurement of muons, the experiments are equipped with approximately one million channels over an area of 10 000 m² of muon chambers. The most sensitive components of the front-end electronics are distributed across the whole detector volume and all the materials and active elements must remain operational after having received the very large radiation doses expected over the lifetime of the experiments. The very selective trigger/DAQ system provides a rejection of approximately 10⁷ in real time. The real and simulated data are handled by large-scale offline software and world-wide connected computing facilities.

Time-scale About 25 years will have passed from the first conceptual studies of the LHC (Lausanne 1984 [8]) to solid physics results, which will mark the transition of the high-energy frontier from the Tevatron to the LHC, presumably in 2010. For many scientists, this period will have represented a major chunk of their professional life and career.

Size of collaboration The number of authors of the first physics papers will have jumped from ~ 600 for the LEP and Tevatron experiments to two to three thousand for ATLAS and CMS. The amount of information circulated and meetings occurring regularly is staggering but appears to be necessary for the collaborations to manage their own work and evolution.

Table 1. For a few physics processes among those expected to be the most abundantly produced at the LHC, expected numbers of events recorded by ATLAS and CMS for an integrated luminosity of 1 fb⁻¹ per experiment [9].

Physics processes	Number of events per fb ⁻¹
QCD jets with $E_T > 150$ GeV	10 ⁶ (for 10% of trigger bandwidth)
$W \rightarrow \mu\nu$	7×10^6
$Z \rightarrow \mu\mu$	1.1×10^6
$t\bar{t} \rightarrow e/\mu + X$	1.6×10^5
$\tilde{g}\tilde{g}$ production ($m_{\tilde{g}} \approx 1$ TeV)	10 ² to 10 ³

2.2. The experimental challenge at the LHC

The LHC represents the next major step in the high-energy frontier beyond the Fermilab Tevatron (proton-antiproton collisions at a centre-of-mass energy of ~ 2 TeV). The high design luminosity is required because of the small cross-sections expected for many of the benchmark processes used to optimise the design of the general-purpose detectors over the past 15 years or so. The cross-sections and expected event rates for processes such as leading Standard Model (SM) processes, Higgs-boson production, supersymmetry, etc., are shown in figure 1 as a function of \sqrt{s} and in table 1 as expected rates at $\sqrt{s} = 14$ TeV for an integrated luminosity of 1 fb^{-1} per experiment. To achieve such luminosities and minimise the impact of inelastic collisions occurring simultaneously in the detectors (a phenomenon known as pile-up), the LHC beam crossings are 25 ns apart in time, resulting in 23 inelastic interactions on average per crossing at design luminosity.

In order to cope with the potentially overwhelming SM processes, high rejection power is needed with optimal efficiency for rare channels such as many of the Higgs-boson decays. In the most extreme case, a selection power of $10^{-14} - 10^{-15}$ is required for Higgs-boson discovery when small signal rates are compared to the total interaction rate. This represents an increase of many orders of magnitude over the selection rates achieved at the Tevatron to-date.

The QCD jet production cross-section is overwhelmingly dominant over all electroweak processes: this means that lepton signatures are most often essential in extracting rare processes from the background at the LHC. It is for this very reason that both excellent measurements and superb identification capabilities of both electrons and muons have been among the primordial requirements of both ATLAS and CMS since the very early design days. Additional signatures have also driven the global design to a large extent, e.g. missing transverse energy, E_T^{miss} , typically indicating the presence of high- p_T non-interacting particles such as neutrinos, or secondary vertices, typically indicating the presence of heavy-flavour hadrons usually embedded in high- p_T b/c -jets.

In addition to the physics challenge itself, the LHC experiments have had to face an even more daunting challenge from the very beginning, namely that of the unprecedented radiation levels expected at design luminosity. At the LHC, the primary source of radiation at design luminosity comes from collisions at the interaction point. In the inner detector, charged hadrons from inelastic proton-proton interactions dominate the radiation backgrounds at small radii, while other sources, such as neutrons, become more important at larger radii, typically above 50 cm.

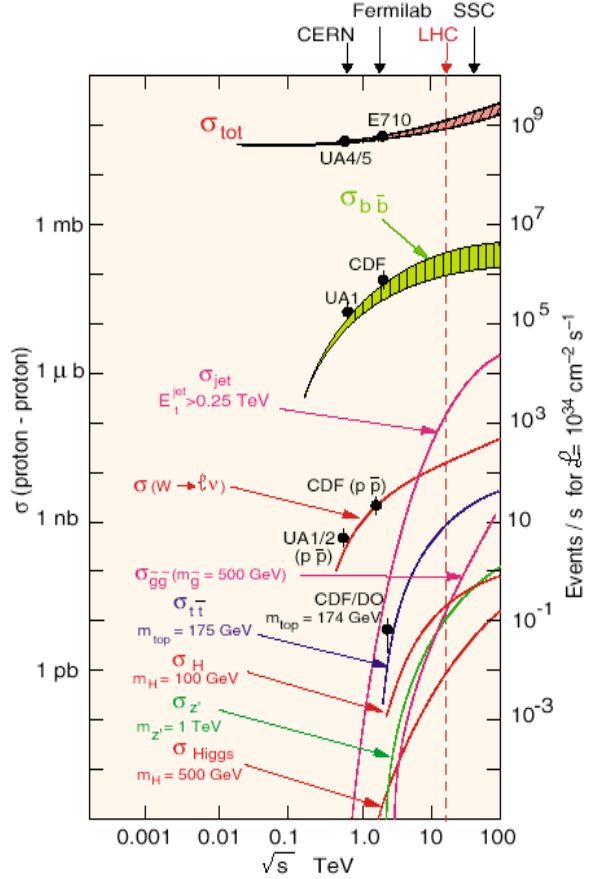


Figure 1. Cross sections and event rates at design luminosity for hard scattering processes as a function of the centre-of-mass energy \sqrt{s} [10].

In this context, the generic features required of the ATLAS and CMS detectors and embodied in their global design are the following:

Detector survival for at least 10 years of operation The high radiation levels will damage the detectors themselves as well as their electronics components. Near the interaction point, in particular, many years of research and development have been spent on selecting the materials, designing front-end electronics, and certifying assembled parts in nuclear reactors and under high ionising radiation, before construction could begin in earnest. The problem of detector survival pervades the whole experimental area at the LHC, because of the high neutron fluences produced in the forward regions where most of the beam energy is dissipated.

Precise timing and fast detector response The bunch-crossing interval of 25 ns provides a direct requirement in this area: in 25 ns, even a relativistic particle only travels a distance of 7.5 m across the detector, whereas the corresponding electronics signals only travel a distance of 5 m out of the typically ~ 100 -metre-long readout cables. These numbers only hint at the massive effort which had to be put into accurate and absolutely reliable timing and control signals throughout the front-end electronics and the trigger system. The source of these timing signals is a single precision clock synchronised with the LHC beams. The speed of the detector response is another requirement which can be met in certain technologies but not in all of them. A slower response means increased sensitivity to out-of-time interactions from preceding or subsequent interactions, thereby compounding the problem of pile-up mentioned above.

Fine spatial granularity A very fine spatial granularity is another ingredient to minimise the impact of pile-up events since an interesting signal in a certain region of the detector occurring at a certain time will only be distorted significantly by other particles if they produce both pile-up in time and in space. Considerations such as these, as well as the occupancy in the core of high- p_T jets have driven some of the choices for the granularity of the tracking detectors and electromagnetic calorimetry.

Identification of extremely rare events As already mentioned, excellent lepton identification should be achieved with high efficiency to extract rare signals from the huge QCD backgrounds. For instance, the electron-to-jet ratio at the LHC is $\sim 10^{-5}$ at $p_T \sim 20$ GeV, a factor ~ 100 times worse than at the Tevatron.

The online rejection to be achieved in real time is $\sim 10^7$ and huge data volumes have to be recorded to permanent storage, typically $\sim 10^9$ events of 1 Mbyte size per year.

2.3. Main design choices

The size of the ATLAS and CMS experiments are directly related to the energies of the particles produced. The calorimeters must absorb the energy of electrons of several TeV (approximately 30 radiation lengths, X_0 , corresponding for instance to 18 cm of lead are required) and of pions of similar energies (approximately 11 interaction lengths, λ , corresponding for instance to 2 m of iron are required). The muon spectrometers and tracking detectors must measure precisely the momenta muons up to several TeV, either inside or outside the calorimeters: BL^2 , the product of the magnetic field strength, B , and of the distance, L , traversed by the muon, is a key factor in this case which must be carefully optimised.

The choice of the magnet system has shaped the experiments in a major way. A strong magnetic field is required to measure the momenta and directions of charged particles near the interaction vertex: this is usually provided by a solenoid, bending the particles in the plane transverse to the proton beams. A strong magnetic field is also required to trigger and if possible measure precisely muon momenta outside the calorimeters (muons are the only charged particles not absorbed in calorimeter absorbers).

In the case of ATLAS, two separate magnet systems have been chosen: a small 2 T solenoid for the tracker and huge toroids with large BL^2 for the muon spectrometer. This option offers a large acceptance in polar angle for the muons (thanks to the toroidal field, which extends to large pseudorapidities) and excellent muon momentum resolution even without using the tracker information. The main drawback of this choice is that it has resulted in a very complex and expensive design and construction project to successfully produce a very large-scale toroid magnet system.

In the case of CMS, on the other hand, the collaboration has opted for a very elegant solution with one large 4 T solenoid with an instrumented iron return yoke. This solution provides both excellent momentum resolution using the tracker and adequate triggering capabilities outside the calorimeter with muon stations embedded in the iron return yoke. This design also leads to a more compact experiment. The muon performance is however limited for stand-alone muon measurements (and for the trigger at very high luminosities) and at small angles to the beam, and the sheer size of the coil allows for only limited space for the calorimeters inside it.

One major concern has emerged over the years as the detailed design of the trackers developed and converged towards a complete definition of all materials inside the envelope of the electromagnetic calorimeters: the material budget of the tracking systems is far superior to that of any of the preceding collider experiments (LEP or Tevatron), and it has increased by a factor of 2 to 2.5 from 1994 (approval of the experiments) to now (operational detectors). The amount of material present in the trackers of ATLAS and CMS is shown in figure 2. Even at small pseudorapidities, the amount of material is 3 – 4 times larger than in the LEP experiments and it represents much more than one radiation length at its peak. Electrons therefore lose between 25% and 70% of their energy and 20% to 65% of photons convert into e^+e^- pairs before reaching the electromagnetic calorimeter. This large and inhomogeneous amount of material has to be known to a precision of $\sim 1\%$ X_0 for the most accurate measurements planned at the LHC, for example the measurement of m_W to less than 10 MeV.

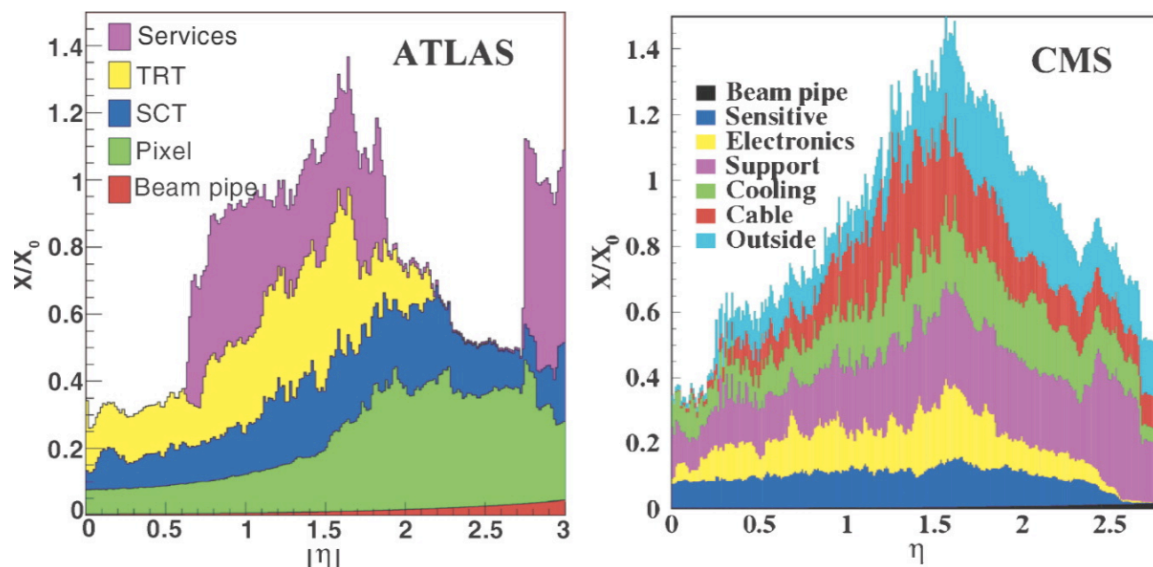


Figure 2. Distribution of amount of material in the volume of the ATLAS (left) and CMS (right) trackers, expressed as fractional radiation length X/X_0 versus pseudorapidity η . These plots do not include additional material just in front of the electromagnetic calorimeters, which is quite large in ATLAS (LAr cryostat and, for the barrel, solenoid coil) and much less in CMS (front part of crystal mechanics) [9].

At the LHC, which is essentially a gluon-gluon collider, the unambiguous identification and precise measurement of leptons is the key to many areas of physics. Electrons are relatively easy to measure precisely in electromagnetic calorimeters but are very hard to identify, as already discussed above. Muons, in contrast, are relatively easy to identify behind the calorimeters, but very hard to measure accurately at high energies. These aspects have also shaped to a large extent the global design and technology choices of the two experiments.

The electromagnetic calorimetry of ATLAS and CMS is based on very different technologies: ATLAS uses a LAr sampling calorimeter with good energy resolution and excellent lateral and longitudinal segmentation, while CMS has chosen PbWO_4 scintillating crystals with excellent energy resolution and lateral segmentation, but without any longitudinal segmentation. Broadly speaking, signals from Higgs-boson decays, such as $H \rightarrow \gamma\gamma$ or $H \rightarrow ZZ^* \rightarrow 4e$, should appear as narrow peaks (intrinsically narrower in CMS) above a fairly pure background from the same final state (intrinsically purer in terms of fakes in ATLAS).

3. Expected performance

3.1. Inner trackers

ATLAS and CMS have designed tracker systems, which provide the same geometrical coverage ($|\eta| < 2.4\text{--}2.5$) and are similar near the interaction vertex, but which differ considerably in terms of the technological choices made at larger radii. The most challenging part of each project, namely the pixel detectors (see figure 3), which surround the interaction point, provide a set of three measurements per primary track at small radii.

At intermediate radii, both trackers contain a set of thin and fine-pitched silicon-strip detectors, providing at least eight (resp. six) measurements per track for ATLAS (resp. CMS), in both the bending plane and along the z -axis through stereo layers.

CMS has extended the silicon-strip technology all the way to the outermost radii, thus providing eight additional measurements per track, with coarser-pitch detectors to cover this large volume. In ATLAS, in contrast, at larger radii, an average of 35 measurements per track in the bending plane are provided by thin straw-tube detectors operating with a Xenon-based gas mixture. The straws are embedded in fibre or foil radiators providing electron identification through absorption of the X-rays from transition radiation, which is produced by highly relativistic particles traversing the multiple interfaces.

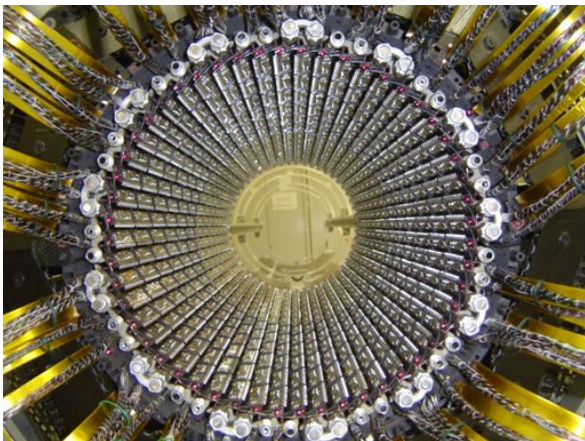


Figure 3. A picture of the ATLAS Pixel innermost layer taken during the pixel barrel integration in 2006.

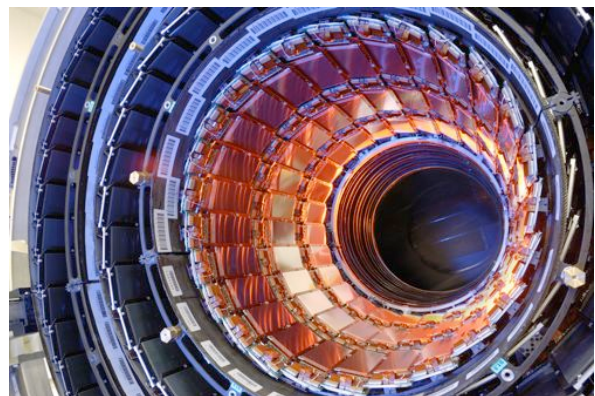


Figure 4. A spectacular view of the interior of one-half of the CMS inner barrel tracker, showing many of the silicon sensors.

Table 2 compares the main performance parameters of the ATLAS and CMS trackers, as obtained from extensive simulation studies performed over the years and benchmarked using detailed test-beam measurements of production modules wherever possible. The unprecedentedly large amount of material present in the trackers is reflected in the overall reconstruction efficiency for charged pions of low transverse momentum, which is only slightly above 80%, as opposed to the value of 97% obtained for muons of the same transverse momentum. The electron track reconstruction efficiency is even more affected by the tracker material, and the numbers shown in table 2 for electrons of 5 GeV transverse momentum are only indicative of the performance expected, as the efficiency obtained depends strongly on the criteria used to define a reasonably well-measured electron track. The somewhat lower efficiencies obtained in the case of CMS are probably due to the higher magnetic field, which enhances effects arising from interactions in the detector material.

Table 2. Main performance characteristics of the ATLAS and CMS trackers: examples of typical reconstruction efficiencies, momentum resolutions, and transverse and longitudinal impact parameter (i.p.) resolutions are given for various particle types, transverse momenta, and pseudorapidities [9].

Tracking properties	ATLAS	CMS
Reconstruction efficiency for pions with $p_T = 1$ GeV	84.0%	80.0%
Reconstruction efficiency for electrons with $p_T = 5$ GeV	90.0%	85.0%
Momentum resolution at $p_T = 100$ GeV and $\eta \approx 0$	3.8%	1.5%
Momentum resolution at $p_T = 100$ GeV and $\eta \approx 2.5$	11%	7%
Transverse i.p. resolution at $p_T = 1000$ GeV and $\eta \approx 0$	11 μm	9 μm
Transverse i.p. resolution at $p_T = 1000$ GeV and $\eta \approx 2.5$	11 μm	11 μm
Longitudinal i.p. resolution at $p_T = 1000$ GeV and $\eta \approx 0$	90 μm	22–42 μm
Longitudinal i.p. resolution at $p_T = 1000$ GeV and $\eta \approx 2.5$	190 μm	70 μm

The performance of the CMS tracker is undoubtedly superior to that of ATLAS in terms of momentum resolution and longitudinal impact parameter resolution. The overall vertexing and b -tagging performances of the two experiments are similar. The impact of the tracker material and of the B -field is however already visible on the individual efficiencies, perhaps more so in CMS. The ATLAS and CMS trackers are expected to deliver performances close to those specified at the time of their conceptual design fifteen years ago, despite the harsh environment in which they will operate for many years and the difficulty of the many technical challenges encountered along the way. In contrast to most of the other systems in the two experiments, however, they will not survive nor deliver the required performance if the LHC luminosity is upgraded to 10^{35} $\text{cm}^{-2}\text{s}^{-1}$. The ATLAS and CMS trackers will therefore have to be replaced by detectors with finer granularity and with an order of magnitude higher resistance to radiation to meet the challenges of the SLHC.

3.2. Electromagnetic calorimetry

The ATLAS and CMS electromagnetic (EM) calorimeters are each divided into a barrel part covering approximately $|\eta| < 1.5$ and two end-caps covering $1.4 < |\eta| < 2.5$ (resp. 3.0) for ATLAS (for CMS). The fiducial coverage of these calorimeters is without appreciable cracks, except perhaps in the transition region between the barrel and end-cap cryostats in the case of ATLAS, where the measurement accuracy is degraded because of large energy losses in the material in

front of the active EM calorimeter. The excellent uniformity of coverage is due to the accordion-shaped electrodes and absorbers of the ATLAS Pb/LAr sampling calorimeter. In CMS, this is obtained by the rotation of the CMS PbWO₄ crystals away from a purely projective arrangement. The total thickness of the EM calorimeters varies from 24 X_0 to 35 X_0 . This depth is sufficient to contain EM showers at the highest energies (a few TeV) and thereby preserve the energy resolution, in particular the constant term, which is dominant above a few hundred GeV.

Figure 5 shows an example of the expected precision with which ATLAS and CMS will perform photon energy measurements. For ATLAS, results are shown for unconverted and converted photons together and for a few typical values of η , over the energy range from 20 to 200 GeV. For CMS, the results are shown for predominantly unconverted photons in the barrel crystal calorimeter and in the energy range from 20 to 110 GeV. For a photon energy of 100 GeV, the ATLAS energy resolution varies between 1.0% and 1.4% over the full η -range. These numbers increase respectively to 1.2% and 1.6% if the expected global constant term of 0.7% is included. The overall expected CMS energy resolution in the barrel crystal calorimeter is 0.75% for the approximately 70% of well-measured photons at that energy before including the expected global constant term of 0.5%. This example shows that the intrinsic resolution of the CMS crystal calorimeter is harder to obtain with the large amount of tracker material in front of the EM calorimeter and in the 4 T magnetic field: between 20% and 60% of photons in the barrel calorimeter acceptance convert before reaching the front face of the crystals.

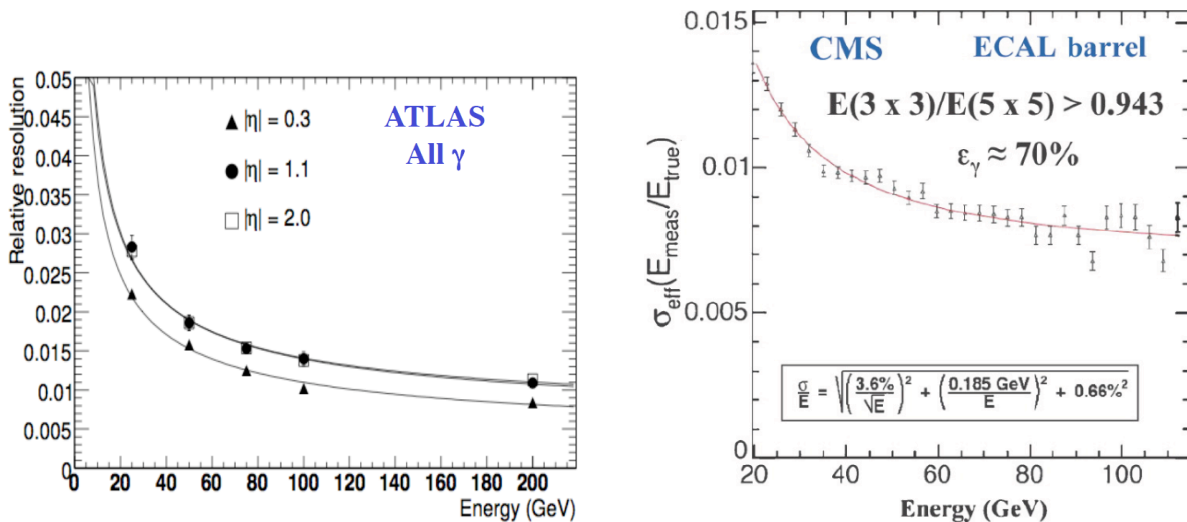


Figure 5. For ATLAS (left) and CMS (right), expected relative precision on the energy measurement of photons as a function of their energy. Also shown are fits to the stochastic, noise, and local constant terms of the calorimeter resolution.

Similarly, figure 6 shows an example of the expected precision with which ATLAS and CMS will perform electron energy measurements. For ATLAS, results are shown for a few typical values of η over the energy range from 10 to 200 GeV. The energy of the electrons is always collected in a 3×7 cell matrix, which is wider in the bending direction to collect as efficiently as possible the bremsstrahlung photons while preserving the linearity and low sensitivity to pile-up and noise. For CMS, the effective resolution (r.m.s. spread) is shown for the barrel crystal calorimeter and in the most difficult low-energy range from 5 to 50 GeV. Refined algorithms are used, in both the tracker and the calorimeter, to recover as much as possible the bremsstrahlung tails and to restore thus most of the excellent intrinsic resolution of the crystal calorimeter. For electrons of 50 GeV, the ATLAS energy resolution varies between 1.5% and 1.8% over the

η -range, without any specific requirements on the performance of the tracker at the moment. In contrast, the CMS effective resolution is estimated to be 2%, demonstrating that it is more difficult in the actual experiment to reconstruct electrons than photons with a performance in terms of efficiency and energy resolution similar to the intrinsic one obtained in test-beam.

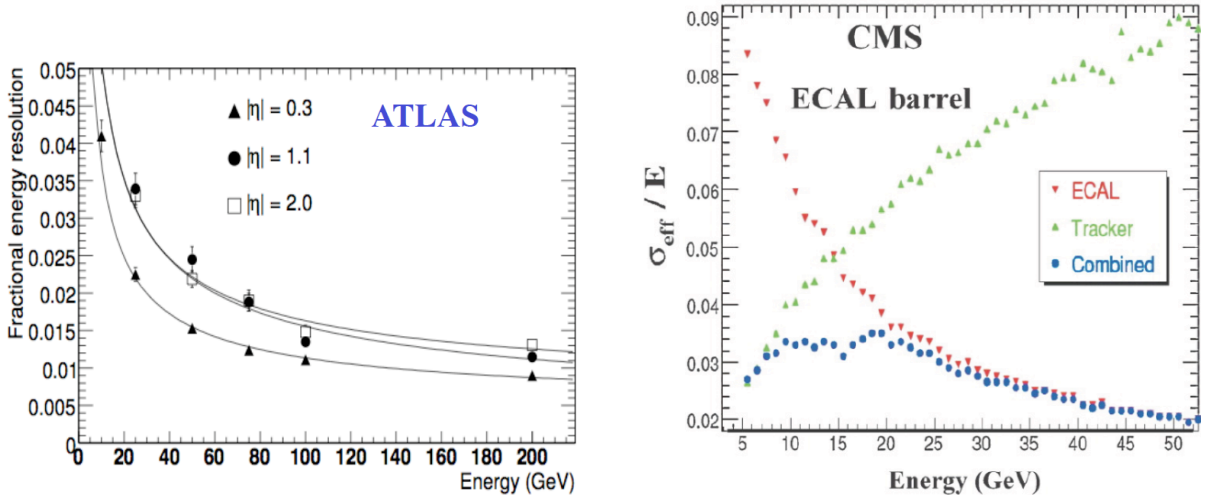


Figure 6. For ATLAS (left) and CMS (right), expected relative precision on the energy measurement of electrons as a function of energy. The resolutions are shown for ATLAS for a few typical values of η together with fits to the stochastic and local constant terms of the calorimeter resolution. For CMS, the combined effective resolution at low energy is shown over the acceptance of the barrel crystal calorimeter, together with the individual contributions from the tracker and the EM calorimeter.

3.3. Hadronic calorimetry

The ATLAS and CMS hadronic calorimeters display a number of significant differences in their design parameters. The strong constraints imposed by the CMS solenoid have resulted in a barrel hadronic calorimeter with an insufficient absorption length of 7.2λ at $\eta = 0$ for the complete calorimeter including the crystals before the coil, so a tail catcher has been added around the coil to complement the calorimetry and to provide better protection against punch-through to the muon system. Consequently, the sampling fraction in the CMS hadronic calorimetry is approximately three times worse than that in the ATLAS hadronic calorimetry, which explains to a great extent the better hadronic resolution expected in ATLAS.

The expected performance for reconstructing hadronic jets is shown in figure 7. Jets are found using a simple cone algorithm with a fixed size in pseudorapidity-azimuth space, so that all cells within a distance $\Delta R = \sqrt{\Delta\eta^2 + \Delta\phi^2}$ of a seed cell are included. For ATLAS, the jet energy resolution is depicted for two η -regions and two different cone sizes over an energy range from 30 to 1000 GeV. The jet energy resolution is shown using a sophisticated weighting technique inspired by the work done in the H1 collaboration. For CMS, the jet energy resolution is shown for a cone size of $\Delta R = 0.5$ and for $|\eta| < 1.4$, over a transverse energy range from 15 to 800 GeV. For completeness, figure 7 also displays the results of fits to the stochastic, noise, and local constant terms of the calorimeter resolutions. For hadronic jets of typically 100 GeV energy, characteristic of jets from W-boson decay, the ATLAS energy resolution in the barrel region is approximately 8%, whereas the CMS energy resolution is approximately 14%.

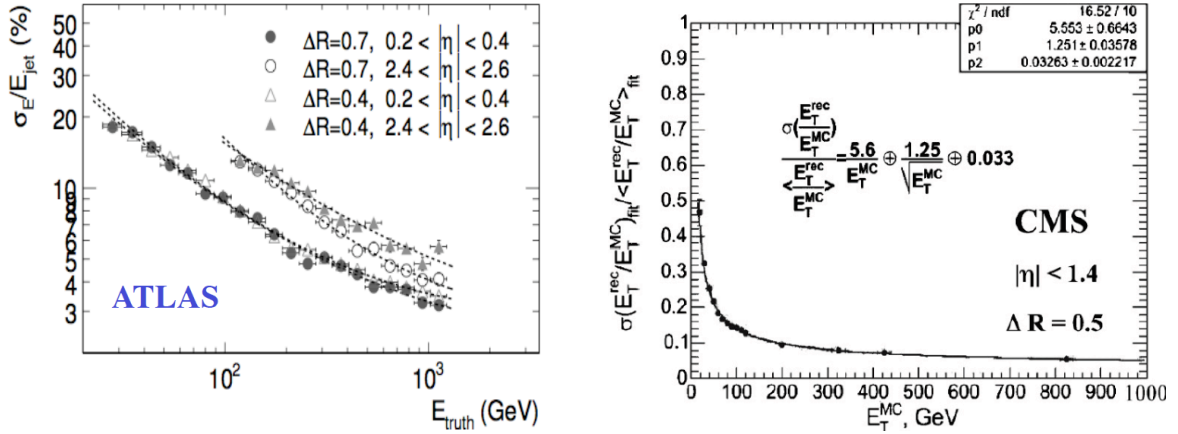


Figure 7. Expected relative precision on the measurement of the reconstructed energy of QCD jets as a function of the jet energy and for two η -ranges for ATLAS (left), and as a function of E_T^{MC} , where E_T^{MC} is the jet transverse energy, in the barrel region for CMS (right).

Finally, figure 8 illustrates an important aspect of the overall calorimeter performance, namely, the expected precision with which the missing transverse energy in the event can be measured in each experiment as a function of the total transverse energy deposited in the calorimeter. The results are expressed as variances of Gaussian fits to the (x, y) components of the missing transverse energy vector, for events from high- p_T jet production and for $A \rightarrow \tau\tau$ decays in ATLAS. For CMS, where the distributions are non-Gaussian, the results are expressed as the r.m.s. of the same distributions for events from high- p_T jet production. For transverse momenta of the hard-scattering process ranging from 70 to 700 GeV, the reconstructed ΣE_T ranges from approximately 500 GeV to approximately 2 TeV. The difference in performance between ATLAS and CMS is a direct consequence of the difference in performance already expected for the jet energy resolution.

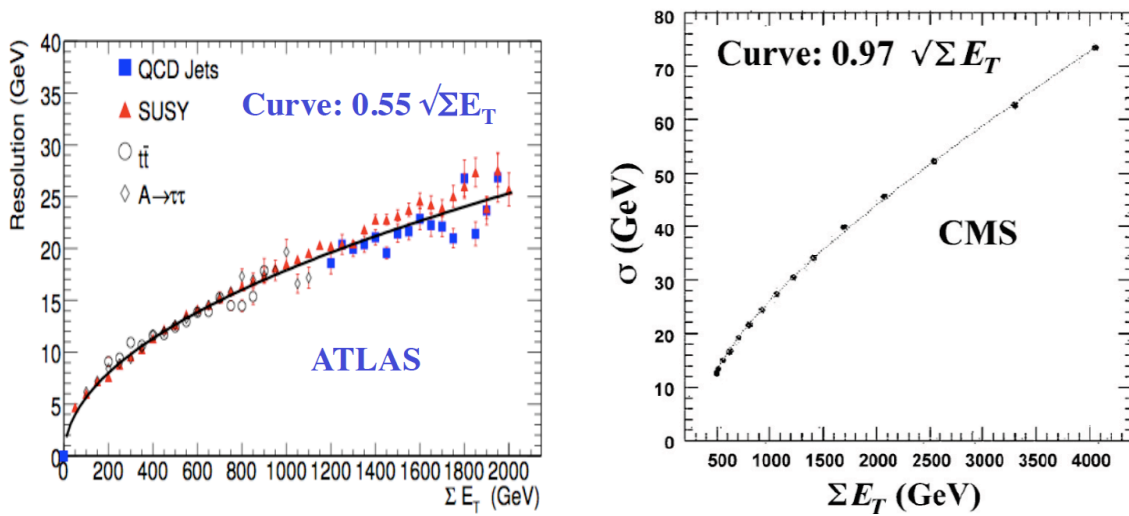


Figure 8. For ATLAS (left) and CMS (right), expected precision on the measurement of the missing transverse energy as a function of the total transverse energy, ΣE_T , measured in the event.

One word about neutrinos in hadron colliders: since most of the energy of the colliding protons escapes down the beam pipe, one can only use the energy-momentum balance in the transverse plane. Therefore, concepts such as E_T^{miss} , missing transverse momentum and mass are often used (the only non-measurable component is E_z^{miss}). These observables allow the complete reconstruction of certain topologies with neutrinos, e.g. $W \rightarrow \ell\nu$ and more importantly $Z/H \rightarrow \tau\tau \rightarrow \ell\nu_\ell\nu_\tau h\nu_\tau$. The experiments must therefore be quite hermetic, so that the transverse energy flow can be fully measured with reasonable accuracy and no neutrino escapes undetected.

3.4. Muon spectrometers

The ability to trigger and reconstruct muons at the highest luminosities of the LHC was incorporated into the design of the ATLAS and CMS detectors from the beginning. In fact, the concepts chosen by the two experiments for measuring muon momenta have shaped the two detectors more than any other physics consideration and, as discussed in Section 2.3, the choice of magnet was motivated by the measurement method of muons with TeV-scale momenta.

The ATLAS toroidal magnetic field provides a momentum resolution that is essentially independent of pseudorapidity up to a value of 2.7. ATLAS has opted for a high-resolution, stand-alone measurement independent of the rest of the subdetectors, resulting in a large volume with low material density over which the muon measurement takes place. The muon system consists of three large superconducting air-core toroid magnets, which are instrumented with different types of chambers to provide two necessary functions, namely, high-precision tracking and triggering. In the central region ($|\eta| < 1.0$), covered by a large barrel magnet consisting of eight coils surrounding the HCAL, tracks are measured in chambers arranged in three cylindrical layers around the beam axis. In the end-cap region, $1.4 < \eta < 2.7$, muon tracks are bent in two smaller end-cap magnets each inserted into one end of the barrel toroid. The transition region, $1.0 < \eta < 1.4$, is less straightforward because here the barrel and end-cap fields overlap, thus partially reducing the bending power. To keep a uniform resolution in this region, tracking chambers, which allow corrections for the change in the magnetic field, are strategically placed.

CMS, on the other hand, uses the concept of a compact detector, which therefore needed a high magnetic field to provide enough bending power for the muon measurement. The CMS solenoidal field bends muon tracks in the transverse plane, as displayed in figure 9, effectively adding another point—the primary vertex position, which is expected to be known with high accuracy—to the muon track. The muon system consists of chambers installed between the iron slabs that provide the return yoke for the magnetic field of the solenoid. In the barrel region, the detectors are arranged in cylinders interleaved with the iron yoke. In the end-caps, the chambers are arranged in four disks perpendicular to the beam and in concentric rings, three rings in the innermost station and two in the others.

Table 3 lists the expected resolutions on the muon momentum measurement for the two spectrometers. The expected near independence of the resolution from the pseudorapidity in ATLAS and the degradation of the resolution at high η in CMS are clearly visible. The resolution of the combined measurement in the barrel region is better in CMS owing to the higher resolution of the measurement in the tracking system, whereas the reverse is true in the end-cap region for high muon momenta owing to the better coverage of the ATLAS toroidal system at large pseudorapidities.

To recapitulate, the actual muon spectrometer performances match that expected from the original designs. The CMS muon spectrometer provides superior combined momentum resolution in the central region, but the stand-alone resolution and trigger at very high luminosities is limited due to multiple scattering in the iron. The overall resolution is degraded in the forward regions ($|\eta| > 2.0$), where the solenoid bending power becomes insufficient. The ATLAS muon spectrometer exhibits excellent stand-alone capabilities and coverage in an open geometry. However the complicated geometry and field configuration results in large fluctuations in

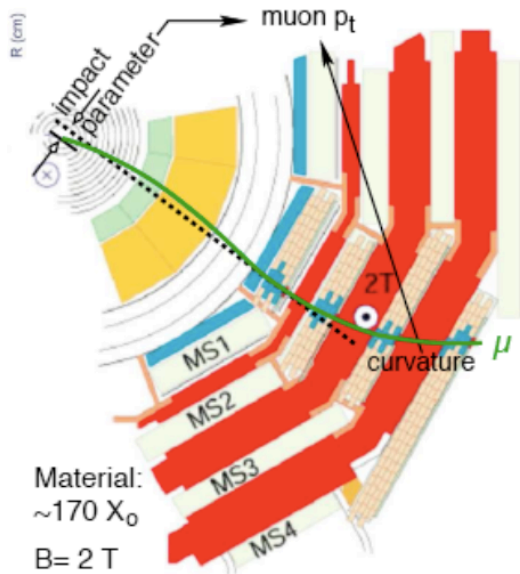


Figure 9. A schematic view of a slice of the CMS detector in the transverse plane. The magnetised iron is in red/dark-grey, and the track trajectory (green solid line) is measured in the inner tracker (hatched circles inside the blue-yellow/light-grey calorimeter) and in the pink/light-grey (blue/dark-grey those hit by the track) muon chambers. Charged particle tracks are bent one way in the tracker and then the other way outside it.

Table 3. Summary of the expected combined and stand-alone (in parenthesis) muon momentum resolution at two typical pseudorapidity values (averaged over azimuth) and for various momentum values [9].

Momentum and pseudorapidity	ATLAS	CMS
$p = 10 \text{ GeV}$ and $\eta \approx 0$	1.4% (3.9%)	0.8% (8%)
$p = 10 \text{ GeV}$ and $\eta \approx 2$	2.4% (6.4%)	2.0% (11%)
$p = 100 \text{ GeV}$ and $\eta \approx 0$	2.6% (3.1%)	1.2% (9%)
$p = 100 \text{ GeV}$ and $\eta \approx 2$	2.1% (3.1%)	1.7% (18%)
$p = 1000 \text{ GeV}$ and $\eta \approx 0$	10.4% (10.5%)	4.5% (13%)
$p = 1000 \text{ GeV}$ and $\eta \approx 2$	4.4% (4.6%)	7.0% (35%)

acceptance and performance over the full potential $\eta \times \phi$ coverage. The CMS muon performance is driven by its tracker, so it is better than ATLAS at $\eta \approx 0$, while the ATLAS muon stand-alone performance is excellent over the whole pseudorapidity range ($|\eta| < 2.7$).

4. Experience with cosmic rays and first beams

During the last two years (2007 and 2008), the focus of the ATLAS and CMS commissioning efforts has evolved from single detector operation to combined running and integration. Several combined tests with cosmic rays have been scheduled to integrate detector, trigger and data acquisition into one global setup for each group of sub-systems (calorimeters, muon detectors, inner detector and magnets). These tests have been very helpful in the commissioning of the subsystems, in the integration of controls and of the trigger and data acquisition. The amount of cosmic data collected by the ATLAS detector versus time is displayed in figure 10.

A central role in the comprehensive pre-collision commissioning campaign was played by the Magnet Test and Cosmic Challenge (MTCC) for the CMS experiment. The objective of the MTCC was the recording, offline reconstruction, and display of cosmic muons in the four subsystems of CMS (tracker, ECAL, HCAL and muon detector) with the magnet operating at its full strength of 4 T. During the test, $25 \cdot 10^6$ cosmic triggered events were recorded with the principal subdetectors active, of which $15 \cdot 10^6$ events have a stable field of $\geq 3.8 \text{ T}$. Data-taking

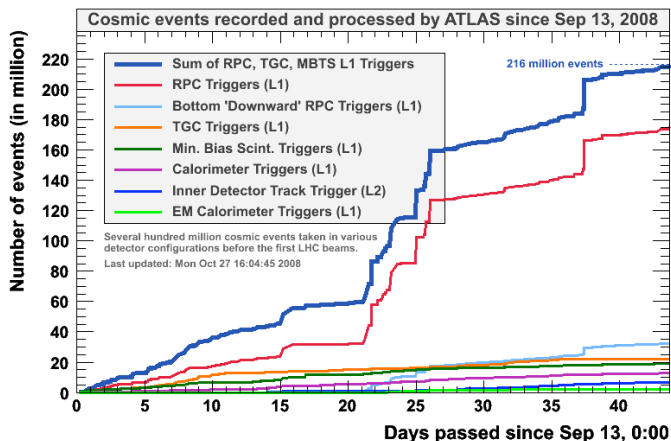


Figure 10. Integrated cosmic data rate for ATLAS versus time after September 13th, 2008, i.e., after the single-beam runs.

efficiency reached over 90% for extended periods. Several thousand of these events correspond to the ‘4-detector’ benchmark, and the whole data sample provided useful understanding and calibration of the combined detector and software performance.

An example of the performance evaluation during the cosmics run can be seen in figure 11 for the ATLAS Transition Radiation Tracker (TRT). The turn-on of the transition-radiation X-ray emission is nicely seen and the identical behaviour of the detector to cosmic tracks and data recorded at the test beam demonstrates that the TRT is working properly. The correspondence between μ^+ and μ^- is very good, and the results achieved with the barrel TRT and the endcap TRT also look much alike.

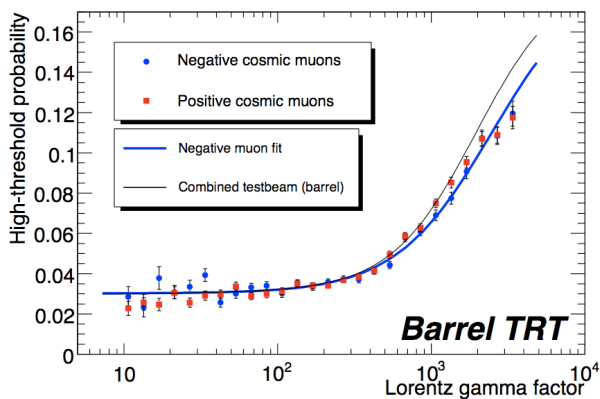


Figure 11. Production of transition-radiation photons as a function of γ as measured for muon tracks during cosmic data taking of the ATLAS TRT in October 2008. The data points, shown for both muon charges (positive: red squares, negative: blue circles), are fitted (thick blue line) and are compared to the results obtained in the ATLAS Combined Test Beam in 2004 (thin black line).

On September 10th, 2008, and later on for few days, LHC have successfully circulated the first proton beams with a single bunch. For safety considerations, ATLAS has taken the data with Pixel detector was switched off, and some other subsystems were operated with reduced voltage. The solenoid magnet was off, but the toroid systems were operational. The beam intensity recorded on September 12th, 2008 during a coast of more than 20 minutes of beam 2 is shown in figure 12. The relative precision determined from the scatter of data points is 10%. The absolute intensity value is not calibrated yet and corresponds roughly to unit of 10^{10} protons. In figure 13, a so-called ‘splash’ event is displayed, as debris of particles hitting the collimator blocks around 150 m from LHC Point 5 deposit energy on the CMS hadronic calorimeter.

More details on the commissioning efforts of ATLAS and CMS can be found in references [11] and [12], respectively, and in references therein.

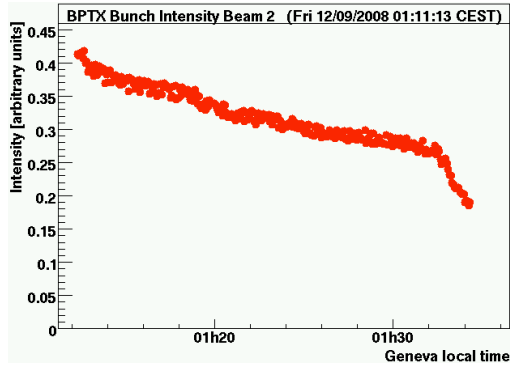


Figure 12. Bunch intensity measured by the beam pick-up monitoring system on September 12th, 2008.

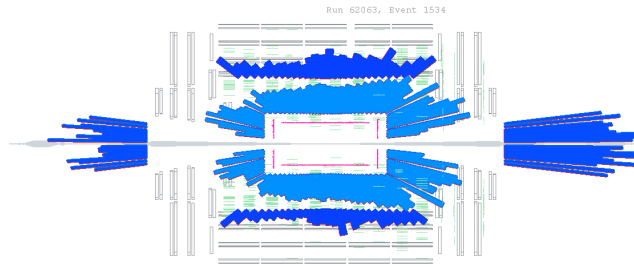


Figure 13. Longitudinal view of the energy deposited in the CMS HCAL calorimeter in a splash event.

5. Early physics: a few examples

As the two LHC experiments start accumulating collision data, it will be possible to probe various aspects of Standard Model and explore new physics scenarios. According to the current schedule of the machine, shown in table 4, the first delivered luminosity will be around $10^{30} \text{ cm}^{-2}\text{s}^{-1}$. Even with a few tens of pb^{-1} expected by the end of 2009, many interesting results can be obtained as will be shown in the following. The main point is that the $\mathcal{O}(10 \text{ TeV})$ energy regime is going to be uncharted territory for particle physics. This is clearly demonstrated in figure 14, where the inclusive jet cross section for the LHC ($\sqrt{s} = 14 \text{ TeV}$) is compared to that of the Tevatron Run I ($\sqrt{s} = 1.8 \text{ TeV}$). However, early data analysis will focus mostly on SM processes with two goals: (i) understanding the performance of complex detectors such as ATLAS and CMS; and (ii) measuring basic SM processes and comparing to theory and various Monte Carlo tools. The expected physics performance for the ATLAS and CMS experiments has been documented in detail in references [13] and [14], respectively.

Table 4. The expected LHC operation parameters in terms of centre-of-mass energy and collected integrated luminosity (as of December 2008).

Year:	2009	2010	2010–2012	> 2012
$\int Ldt/\text{yr}$	10–100 pb^{-1}	0.5–2 fb^{-1}	$\mathcal{O}(10 \text{ fb}^{-1})$	$\mathcal{O}(100 \text{ fb}^{-1})$
Energy	8–10 TeV	14 TeV	14 TeV	14 TeV

The available collision data will be completely dominated by minimum bias and QCD jet events, as shown in figure 14. This will allow the study of the underlying event using minimum bias and di-jet samples and the tuning of the relevant Monte Carlo generators. Besides that, and despite the theoretical uncertainties on the QCD production at these energies, search for new phenomena will be feasible. For example, contact interactions will be accessible during the first year of LHC operation. As demonstrated in figure 15, contact interactions induce large rates on high- p_T jets. The experimental error will be dominated by the jet energy scale ($\sim 10\%$) during early running, however this will not compromise the discovery potential for $p_T > 1 \text{ TeV}$ at $\Lambda^+ = 3 \text{ TeV}$ [15]. This means that even with only 10 pb^{-1} the current bound of $\Lambda^+ > 2.7 \text{ TeV}$ set by Tevatron can be superseded.

The cross-sections for various physics processes producing isolated leptons at the LHC are

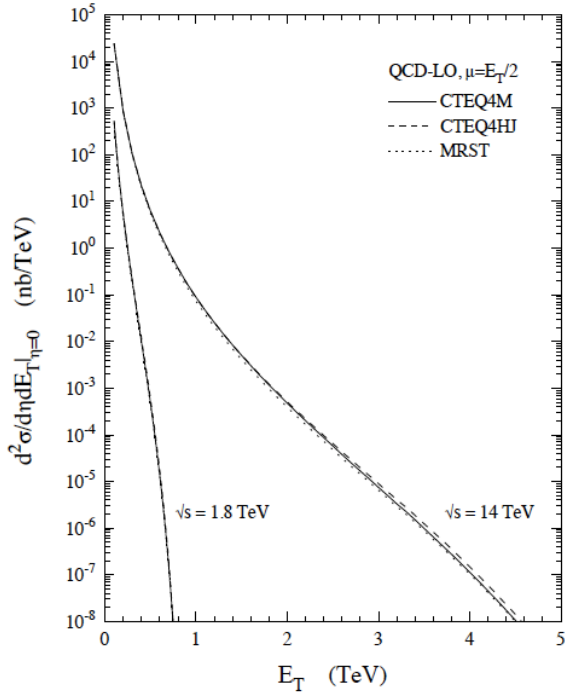


Figure 14. The inclusive jet cross sections at a rapidity of $\eta = 0$ for both the Tevatron and the LHC [16].

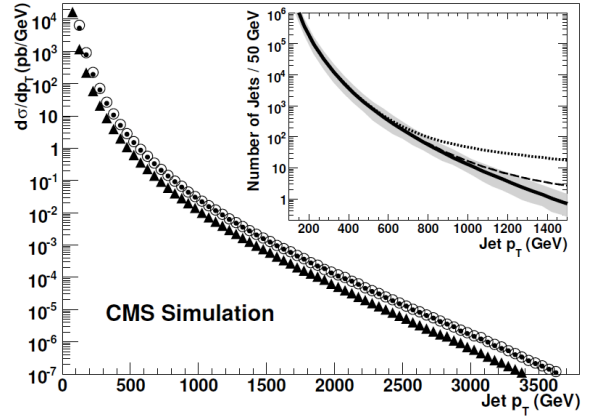


Figure 15. The inclusive jet p_T differential cross section expected from QCD, for generated jets (points), reconstructed jets (triangles), and corrected jets (open circles). The inset shows the number of generated jets expected for 10 pb^{-1} . The standard QCD curve (solid) is modified by a signal from contact interactions with scale $\Lambda^+ = 3 \text{ TeV}$ (dotted) and 5 TeV (dashed). The shaded band represents the effect of a 10% uncertainty on the jet energy scale. [15].

quite large. Taking electrons in ATLAS as an example, for an integrated luminosity of 100 pb^{-1} , one expects to trigger and reconstruct on roughly 250 000 J/ψ , $10^6 W \rightarrow e\nu$ and 50 000 $Z \rightarrow ee$ decays. For early data, the single (resp. double) electron trigger thresholds range from 10 to 20 GeV (resp. 5 to 15 GeV), and the collection of large samples of isolated electrons will be possible rapidly, a crucial element for the understanding of the initial detector and trigger performance.

Similarly to electrons, the detection and measurement of di-muons will provide an excellent opportunity to collect large samples to understand the performance of the relevant detectors and trigger. The invariant mass of the di-muons for the two most prominent states from low-mass resonances are displayed in figure 16. After all selection cuts, ATLAS will record about 4200 (resp. 800) events from J/ψ (resp. Υ) decays to a muon pair per day at a luminosity of $10^{31} \text{ cm}^{-2}\text{s}^{-1}$, assuming an overall 30% machine and detector data-taking efficiency. These events will provide quantitative information on the tracker momentum scale, on the trigger performance, the individual detector efficiencies, etc. However, care will have to be devoted to minimise and control the backgrounds from heavy flavours and π/K decays.

High-mass resonances such as the Z peak will also provide crucial information. After all cuts, about 160 $Z \rightarrow \mu\mu$ events per day are expected to be observed with a luminosity of $L = 10^{31} \text{ cm}^{-2}\text{s}^{-1}$. This corresponds to a rate for Z events 10 times higher than the Tevatron. The precision on the $Z \rightarrow \mu\mu$ cross section measurement is limited with 100 pb^{-1} by $< 2\%$ experimental errors, such as mis-alignment of the muon spectrometer (see figure 17) and by $\sim 10\%$ by the luminosity error. These studies are expected to aid at the muon spectrometer alignment and at the determination of the EM calorimeter uniformity and the energy/momentum scale of the full detector. The intercalibration of the EM and the hadronic calorimeter using azimuthal symmetry is also possible. Additionally, the lepton trigger and reconstruction

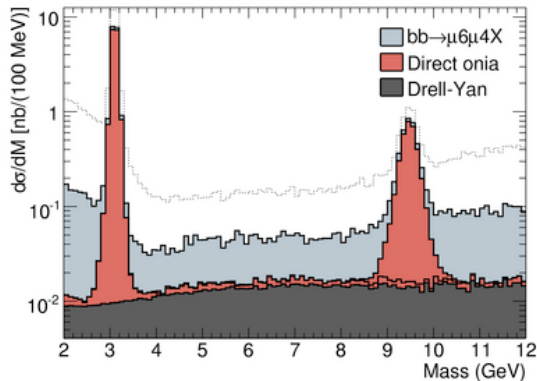


Figure 16. Distribution of di-muon invariant mass in the region of the J/ψ and Υ resonances in ATLAS, shown above the backgrounds from heavy-flavour and Drell-Yan production.

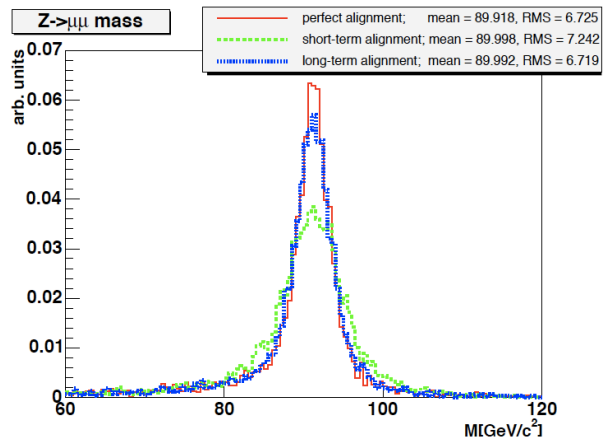


Figure 17. Z mass reconstruction from di-muons in CMS for various (mis)alignment scenarios [17].

efficiency will be better understood.

The first top quarks outside Fermilab will be seen at the LHC. The top-pair signal in the semi-leptonic channel can be extracted using event counting or the three-jet invariant distribution. The latter is demonstrated in figure 18. A signal can be established with 100 pb^{-1} even if a pessimistic background knowledge is assumed. With this integrated luminosity, the b-tagging is expected to be understood and its efficiency known to $< 5\%$, allowing thus its use in the event selection. By requiring one or two b-jets, the non- $t\bar{t}$ background will be reduced and the selection of the correct combination will be improved. As seen in figure 19, with $\mathcal{O}(1 \text{ fb}^{-1})$ the b-tagging and the knowledge of the parton distribution functions are important, whilst at higher integrated luminosities the error on the luminosity dominates the overall uncertainty.

Obvious candidates for first searches are heavy resonances decaying to leptons. A number of benchmark Z' models has been studied at LHC: the Sequential Standard Model (Z'_{SSM}), the E_6 models Z'_ψ , Z'_χ , Z'_η , and the left-right symmetric model (Z'_{LR}). With 100 pb^{-1} a signal large enough for a 5σ discovery can be observed for masses up to 1 TeV, as seen in table 5. Indicatively, the Tevatron reach for 5σ discovery with 7 fb^{-1} of collected data is $\sim 1 \text{ TeV}$. The ultimate ATLAS reach, with 300 fb^{-1} is expected to be $\sim 5 \text{ TeV}$. The signal can be seen as a (narrow) mass peak on top of the small (at these energies) Drell-Yan background. This is demonstrated in figure 20 for a Z'_χ with a mass of 1 TeV. The ultimate calorimeter performance is not required for these studies, rendering them thus independent of the calorimeter calibration procedures. The di-tau signature is another possibility for the search for high mass resonances. This becomes very important, in particular, in models where a hypothetical new resonance couples preferentially to the third generation [13].

Furthermore, the first LHC data will allow to perform searches for R -parity conserving supersymmetry (SUSY). If it exists at the TeV scale, it should be found ‘quickly’ exploiting the large (strong) production cross sections for $\tilde{q}\tilde{g}$, $\tilde{g}\tilde{g}$ and $\tilde{q}\tilde{q}$. Spectacular signatures, involving many jets, leptons and $E_{\text{T}}^{\text{miss}}$ —due to the (stable) lightest neutralinos escaping the detector without interacting with it—are expected from the cascade decay of superpartners, as shown in figure 21. At the LHC, for $m_{\tilde{q}}, m_{\tilde{g}} \approx 1 \text{ TeV}$, about 10 events/day are expected at $L = 10^{32} \text{ cm}^{-2}\text{s}^{-1}$. Hints for SUSY up to 1 TeV can be seen at the LHC with only 100 pb^{-1} , whilst the 95% C.L. reach at the Tevatron is up to $\sim 400 \text{ GeV}$. The analysis will be based to a

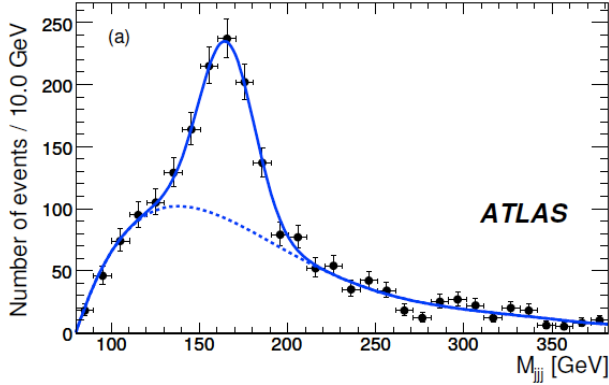


Figure 18. Fit to the three-jet invariant mass in ATLAS for 200 pb^{-1} : the Chebychev polynomial fit to the background (dotted line) and the Gaussian fit of the signal events (full line) are shown [13].

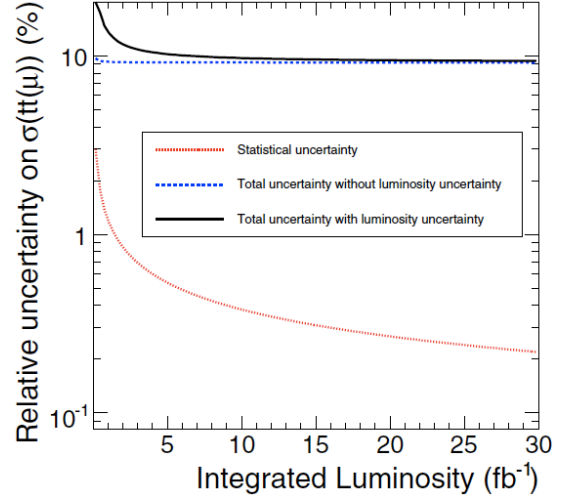


Figure 19. Statistical and total uncertainty on the inferred cross section by CMS of the process $pp \rightarrow t\bar{t} \rightarrow b\bar{q}\bar{q}\mu\nu_\mu$ versus the integrated luminosity [14].

Table 5. Event rate after all analysis cuts and integrated luminosity required for 5σ discovery (corresponding to 10 observed events) for Z'_{SSM} decaying to leptons.

Mass [TeV]	Events / fb^{-1}	$\int Ldt$ [pb^{-1}]
1.0	~ 160	~ 70
1.5	~ 30	~ 300
2.0	~ 7	~ 1500

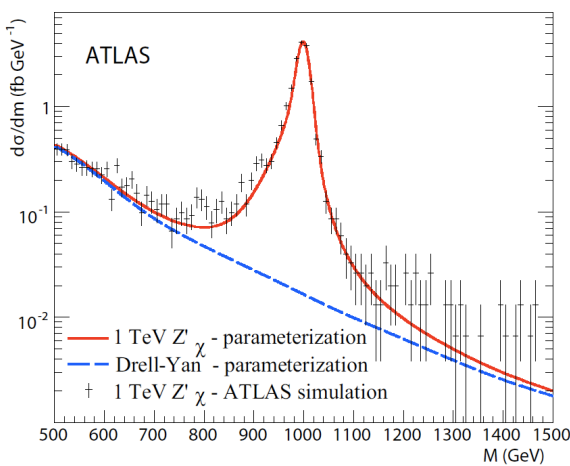


Figure 20. Mass spectrum for a $m = 1 \text{ TeV}$ $Z'_\chi \rightarrow e^+e^-$ obtained with ATLAS full simulation (histogram) and the parameterisation (solid line). The dashed line corresponds to the parameterisation of the Drell-Yan process (irreducible background) [13].

large extent to the high missing energy that characterises the SUSY events, as demonstrated in figure 22. However precise understanding of the relevant backgrounds will require $\sim 1 \text{ fb}^{-1}$. To this respect, R -parity *violating* SUSY may be easier to be probed, since it does not rely on $E_{\text{T}}^{\text{miss}}$ -based selection criteria. In order to bypass the uncertainty on the missing-energy measurement

during the first data taking, various techniques providing data-driven background estimation have been developed [13] for SUSY searches.

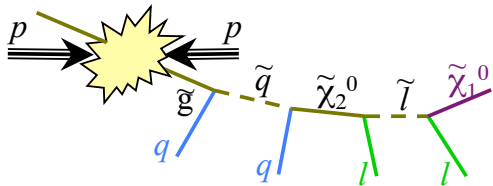


Figure 21. Schematic view of a typical supersymmetric cascade decay at the LHC. The $\tilde{q}\tilde{g}$, $\tilde{g}\tilde{g}$ and $\tilde{q}\tilde{q}$ production processes dominate, whilst the gaugino pair production is suppressed. The other \tilde{g} or \tilde{q} decays in a similar manner (not shown).

The eventual discovery reach of the LHC as a function of the collected integrated luminosity (and time) is summarised in figure 23. A sample of exotic physics scenarios that will be explored at the LHC in the next few years is given below.

Excited quarks They are predicted in composite-quark models. Through their decay to photons, $q^* \rightarrow q\gamma$, they can be probed up to $m \approx 6$ TeV, if the compositeness scale is less than the LHC energy.

Leptoquarks The experimentally observed symmetry between leptons and quarks has motivated the search for leptoquarks, hypothetical bosons carrying both baryon and lepton quantum numbers. Their discovery will be feasible through their pair production up to $m \approx 1.5$ TeV.

Monopoles The existence of Dirac magnetic monopoles will be investigated at the LHC via the production of a photon pair from a virtual monopole loop, $pp \rightarrow pp\gamma\gamma$, for masses $m \lesssim 20$ TeV.

Compositeness If the compositeness scale Λ is much larger than the centre of mass energy of the colliding partons, $\sqrt{s} = 14$ TeV, the manifestation of compositeness will be an effective 4-fermion contact interaction. The angular distributions and rates of high- p_T di-jets and di-muons will allow to probe fermion compositeness up to $\Lambda \approx 40$ TeV.

Heavy resonances New heavy states forming a narrow resonance decaying into opposite sign di-leptons are predicted in many extensions of the Standard Model: grand unified theories, technicolor, little Higgs models, and models involving extra dimensions. Di-lepton and di-jet states, such as $Z' \rightarrow \ell\ell, qq$, will be probed up to $m \approx 5$ TeV, whereas resonances decaying to a lepton and a neutrino ($W' \rightarrow \ell\nu$) will be searched for masses $m \lesssim 6$ TeV.

The opportunities for the discovery of new physics at the LHC are numerous and the ATLAS and CMS detectors have been optimised very systematically towards maximum sensitivity to almost any new physics signals, based on detailed benchmarks from many models. Nevertheless, even some known physics measurements might be beyond the reach of the LHC (and even of

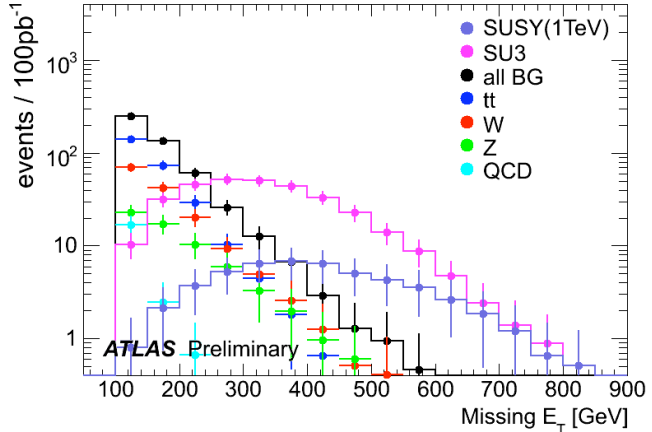


Figure 22. E_T^{miss} distributions for various background processes, for the ATLAS SUSY point SU3 (700 GeV) and for SUSY at 1-TeV scale in the no-lepton mode for an integrated luminosity of 1 fb^{-1} [13].

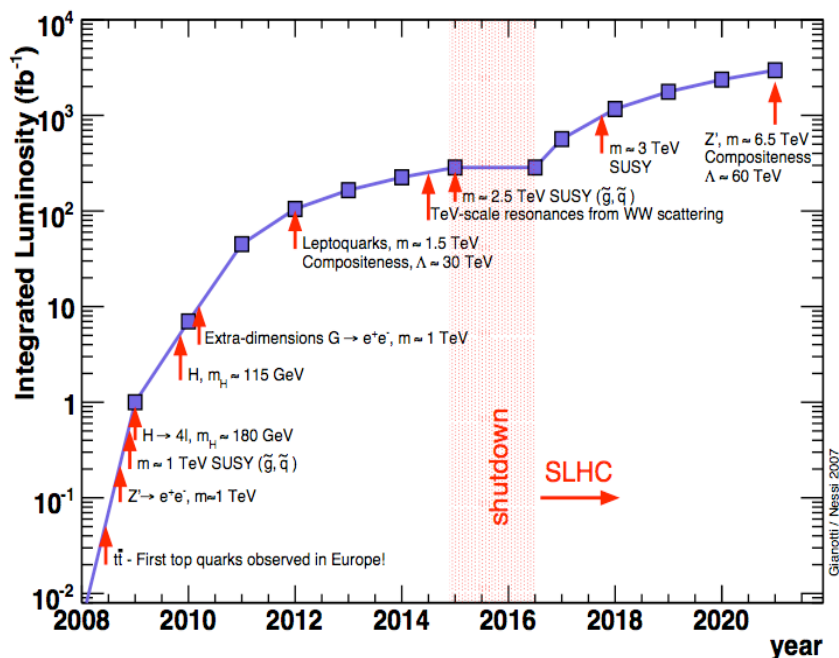


Figure 23. LHC discovery potential versus time and integrated luminosity (Credit: F. Gianotti and M. Nesi, 2007).

the SLHC), such as the Higgs-boson self-coupling and the detection of charginos and neutralinos in many supersymmetry scenarios.

6. Outlook

The LHC accelerator and its experiments represent the front wave of the field of experimental particle physics and it is a wonderful achievement of the community across the whole world that these very challenging projects have all been able to successfully conclude their last phases of installation and commissioning in 2008. These projects have been with us however for almost twenty years and have become gigantic in terms of their complexity, their funding and their human resources. One could argue that the whole project has become dinosaur-like in terms of sheer size and scope.

The most prominent issue with the scope of the LHC experiments is related to the very long time-scales involved which threaten to breach the continuity ensured between generations of experimental and theoretical physicists through rapid turnover between new ideas and concepts, both in theory and technical developments, new experiments, and new physics results, leading in turn to new ideas and concepts. Theory and foremost among all the Standard Model has not been sufficiently challenged nor nourished by experiment for too long (leaving aside in this context the exciting results obtained in neutrino physics over the past ten-fifteen years). Most of the young physicists now joining ATLAS and CMS have no idea of what really has been installed in the experimental halls, nor of how formidable a challenge it has been to build, install and commission these detectors. Very few people remember today that in the late 1980's most experimental physicists believed it would be impossible to operate tracking detectors in the radiation environment of the LHC accelerator.

The stakes of these projects have therefore become very high and it is out of the question nowadays to afford shots in the dark of such a large size and scope. Success must be guaranteed,

if not in terms of physics results, at least in terms of achieved technical goals and detector performance for known physics processes. This also probably means that one can no longer afford, as in the early 1980's, to approve the next large machine before the current one has delivered some results.

On the other hand, this is why the challenge in front of us at the LHC is so exhilarating! A major fraction of the future of our discipline hangs on the physics which will be harvested at this new energy frontier. How ordinary or extraordinary will this harvest be? Only nature knows.

References

- [1] Evans L and Bryant P 2008 LHC machine *J. Instrum.* JINST **3** S08001
- [2] Aad G *et al* [ATLAS Collaboration] 2008 The ATLAS experiment at the CERN Large Hadron Collider *J. Instrum.* JINST **3** S08003
- [3] Adolphi R *et al* [CMS Collaboration] 2008 The CMS experiment at the CERN LHC *J. Instrum.* JINST **3** S08004
- [4] Alves A A *et al* [LHCb Collaboration] 2008 The LHCb detector at the LHC *J. Instrum.* JINST **3** S08005
- [5] Aamodt K *et al* [ALICE Collaboration] 2008 The ALICE experiment at the CERN LHC *J. Instrum.* JINST **3** S08002
- [6] Anelli G *et al* [TOTEM Collaboration] 2008 The TOTEM experiment at the CERN Large Hadron Collider *J. Instrum.* JINST **3** S08007
- [7] Adriani O *et al* [LHCf Collaboration] 2008 The LHCf detector at the CERN Large Hadron Collider *J. Instrum.* JINST **3** S08006
- [8] Asner A *et al.* 1984 Proc. ECFA-CERN Workshop on Large Hadron Collider in the LEP tunnel, 21–27 March 1984, Lausanne and CERN, Geneva, Switzerland *CERN Reports* CERN-84-10-V-1 & CERN-84-10-V-2
- [9] Froidevaux D and Sphicas P 2006 General-purpose detectors for the Large Hadron Collider *Ann. Rev. Nucl. Part. Sci.* **56** 375–440
- [10] Altarelli G and Mangano M L 2000 Proc. CERN Workshop on Standard Model physics (and more) at the LHC, 25–26 May 1999, Geneva, Switzerland CERN-2000-004
- [11] Abat E *et al* 2008 Combined performance tests before installation of the ATLAS Semiconductor and Transition Radiation Tracking Detectors *J. Instrum.* JINST **3** P08003
Costa M J 2009 Commissioning of the ATLAS detector with cosmic rays and first LHC beams *J. Phys.: Conf. Series* to appear
- [12] Acosta D 2008 Status of CMS commissioning *Nuovo Cim.* **123B** 1014
- [13] Aad G *et al* [ATLAS Collaboration] 2008 Expected Performance of the ATLAS Experiment - Detector, Trigger and Physics *CERN Report* CERN-OPEN-2008-020 *Preprint* arXiv:0901.0512
- [14] Bayatian G L *et al* [CMS Collaboration] 2007 CMS technical design report, volume II: Physics performance *J. Phys. G* **34** 995–1579
- [15] Cardaci M, Bollen B, Esen S, Jha, M K, Chlebana F, Harris R M, Kousouris K, Mason D, Zielinski M and Bhatti 2008 CMS search plans and sensitivity to new physics using dijets *CMS Note* CMS-NOTE-2008-019
- [16] Huston J 1999 LHC Guide to Parton Distribution Functions *ATLAS Note* ATL-PHYS-99-008
- [17] Vanlaer P, Barbone L, De Filippis N, Speer T, Buchmüller O and Schilling F P 2006 Impact of CMS Silicon Tracker Misalignment on Track and Vertex Reconstruction *CMS Note* CMS-NOTE-2006-029